Ehtsham Azhar*, Z. Iqbal and E.N. Maraj

Impact of Entropy Generation on Stagnation-Point Flow of Sutterby Nanofluid: A Numerical Analysis

DOI 10.1515/zna-2016-0188
Received May 7, 2016; accepted July 18, 2016; previously published online August 13, 2016

Abstract: The present article dicusses the computational analysis of entropy generation for the stagnation-point flow of Sutterby nanofluid over a linear stretching plate. The Sutterby fluid is chosen to study the effect for three major classes of non-Newtonian fluids, i.e. pseudoplastic, Newtonian, and dilatant. The effects of pertinent physical parameters are examined under the approximation of boundary layer. The system of coupled nonlinear partial differential equations is simplified by incorporating suitable similarity transformation into a system of nonlinear-coupled ordinary differential equations. Entropy generation analysis is conducted numerically, and the results are displayed through graphs and tables. Significant findings are listed in the closing remarks.

Keywords: Entropy Generation; Nanoparticle; Shooting Algorithm (RK-5); Stagnation-Point Flow; Sutterby Fluid.

1 Introduction

In many industries and manufacturing processes, different types of fluids are encountered, such as polymer melts, colloidal suspensions, organic chain mixtures, etc. The Naiver-Stokes equation alone is insufficient to describe the rheological properties of these fluids. Therefore, to depict the rheological properties of complex fluids, many nonlinear fluid models are nominated. The Sutterby fluid model [1] is one of the non-Newtonian fluid models used to analyze the significant properties of pseudoplastic and dilatant fluids. This model has an edge on other models. As for the different values of power law index m, it shows the behavior of the Newtonian fluid, shear thinning, and thickening fluids. That is, when $m=0$, this model deduces from the Newtonian fluid; when $m<0$, it exhibits the properties of pseudoplastic fluids; and when $m>0$, it shows the rheological trends of shear thickening fluids.

The boundary layer flow of non-Newtonian fluids is of immense interest because of its wide application in the extrusion of polymer sheets and emulsion coating, i.e. photographic films, solutions, and melts of high molecular weight polymers. The study of boundary layer flows over a continuous surface was initiated and formulated by Sakiadis [2]. Lyubimov and Perminov [3] examined the Williamson fluid flow over a thin inclined surface in the presence of gravitational field. The boundary layer flow of an Oldroyd-B fluid under the implementation of convective boundaries was investigated by Hayat et al. [4]. The flow of a Williamson fluid over a stretching sheet by applying boundary layer approximation was studied by Nadeem et al. [5]. The flow of a second-grade fluid over a stretching surface with Newtonian heating was analyzed by Hayat et al. [6]. Bidin and Nazar [7] performed a numerical analysis of the boundary layer flow over an exponentially stretching sheet with thermal radiation.

Nanofluids have gained immense importance in the present era in reference to its utility in controlling heat transfer within the system. Choi [8] was the first one to experimentally examine the effect of nanoparticles. Buongiorno [9] contributed mainly in establishing a depth enquire of all feasible ways through which nanoparticles slip during the convection of nanofluids. He concluded that nanofluids contribute in an upsurge of heat transfer coefficient in the turbulent region because of the deviation of thermophysical properties within the boundary layer affected by thermopohoresis and temperature gradient. The Brownian motion and the thermophoresis effect on the slip flow of alumina/water nanofluid inside a circular microchannel in the presence of a magnetic field were examined by Malvandi and Ganji [10].

The stagnation-point flow of a fluid past a stretching sheet has been given much attention in recent times. This is in view of their importance in many industrial applications, such as extrusion, paper production, insulating materials, glass drawing, continuous casting, etc. The stagnation-point flow was first investigated by Hiemenz [11]. Chiam [12] investigated the steady two-dimensional stagnation-point flow of a viscous fluid toward a

***Corresponding author: Ehtsham Azhar,** Department of Mathematics, HITEC University, Taxila, Pakistan,
E-mail: ehtsham@uaar.edu.pk
Z. Iqbal and E.N. Maraj: Department of Mathematics, HITEC University, Taxila, Pakistan

stretching sheet. Khan and Pop [13] studied flow near a two-dimensional stagnation point on an infinite permeable wall with a homogeneous-heterogeneous reaction. Zhong and Fung [14] contributed by exploring unsteady stagnation-point flow over a plate moving along the direction of flow impingement. Stagnation-point flow and heat transfer over an exponentially shrinking sheet were investigated by Bhattacharyya and Vajravelu [15]. The unsteady flow of nanofluid in the stagnation-point region of the time-dependent rotating sphere was analyzed by Malvandi [16]. In another article, Malvandi et al. [17] examined the slip effects on the unsteady stagnation-point flow of a nanofluid over a stretching sheet.

In heat transfer analysis, the measure of disorder is significant for the knowledge of the efficiency of a system. Entropy generation number and irreversibility parameter are helpful in this regard. Entropy generation number depends mostly on two major factors, i.e. heat transfer and viscous dissipation. The entropy generation of nanofluid in helical tube and laminar flow was discussed by Falahat [18]. Jie and Clement [19] analyzed entropy generation for nanofluid flow in microchannels. Hassan et al. [20] performed the numerical study of entropy generation in micro- and minichannels. Mahian et al. [21] gave an experimental review of entropy generation in nanofluid flow. Moreover, an analytical study on the entropy generation of nanofluids over a flat plate was conducted by Malvandi et al. [22]. Few articles are cited [10, 18–29] to give an aerial view on the study of the entropy generation of nanofluids.

Motivated by the above-mentioned studies and applications, the purpose of this paper is to address the effect of the entropy generation stagnation-point flow of Sutterby nanofluid over a linearly stretching sheet. Effects of thermophoresis and Brownian motion are seen carefully. Numerical solutions are derived for the resulting nonlinear analysis. Graphical results for different parameters are discussed. Nusselt and Sherwood numbers are also shown and analyzed. The comparison of numerical values of Nusselt number with the previous results is also reported in the present analysis.

2 Fluid Model

Cauchy stress tensor τ and extra stress tensor $\mathbf{S}$ for the Sutterby fluid are given as [1]

$$\tau = -pI + \mathbf{S}, \tag{1}$$

$$\mathbf{S} = \mu_0 \left[\frac{\sinh B\sqrt{(|\dot{\gamma}|)^2}}{B\sqrt{(|\dot{\gamma}|)^2}} \right]^m |\dot{\gamma}|, \tag{2}$$

in which p is the pressure, I is the identity vector, μ_0 is the viscosity, B is the material constant, and m is the power law index. The definition of $\dot{\gamma}$ is

$$|\dot{\gamma}| = \sqrt{\frac{1}{2}\text{trace}(A_1)^2}, \tag{3}$$

in which

$$A_1 = \nabla V + (\nabla V)^T, \tag{4}$$

$$|\dot{\gamma}| = \left[2\left(\frac{\partial u}{\partial x}\right)^2 + \left(\frac{\partial u}{\partial y} + \frac{\partial v}{\partial x}\right)^2 + 2\left(\frac{\partial v}{\partial y}\right)^2 \right]^{1/2}. \tag{5}$$

The extra stress tensor $\mathbf{S}$ becomes

$$\mathbf{S} = \mu_0 \left[1 + \frac{B^2(|\dot{\gamma}|)^2}{6} \right]^m |\dot{\gamma}|, \tag{6}$$

and by using binomial expansion, we get

$$\mathbf{S} = \mu_0 \left[1 + \frac{mB^2(|\dot{\gamma}|)^2}{6} \right] |\dot{\gamma}|. \tag{7}$$

The components of the extra stress tensor $\mathbf{S}$ are as follows:

$$S_{xx} = 2\mu_0 \left[1 + \frac{mB^2}{6}\left(2\left(\frac{\partial u}{\partial x}\right)^2 + \left(\frac{\partial u}{\partial y} + \frac{\partial v}{\partial x}\right)^2 + 2\left(\frac{\partial v}{\partial y}\right)^2 \right) \right] \left(\frac{\partial u}{\partial x}\right), \tag{8}$$

$$S_{xy} = S_{yx} = \mu_0 \left[1 + \frac{mB^2}{6}\left(2\left(\frac{\partial u}{\partial x}\right)^2 + \left(\frac{\partial u}{\partial y} + \frac{\partial v}{\partial x}\right)^2 + 2\left(\frac{\partial v}{\partial y}\right)^2 \right) \right] \left(\frac{\partial u}{\partial y} + \frac{\partial v}{\partial x}\right), \tag{9}$$

$$S_{yy} = 2\mu_0 \left[1 + \frac{mB^2}{6}\left(2\left(\frac{\partial u}{\partial x}\right)^2 + \left(\frac{\partial u}{\partial y} + \frac{\partial v}{\partial x}\right)^2 + 2\left(\frac{\partial v}{\partial y}\right)^2 \right) \right] \left(\frac{\partial v}{\partial y}\right), \tag{10}$$

$$S_{xz} = S_{yz} = S_{zx} = S_{zy} = S_{zz} = 0. \tag{11}$$

Applying standard boundary layer [2] approximations to the components of tensor, we arrived at

$$\frac{S_{xx}}{\rho}=\frac{2\mu_0}{\rho}\left[1+\frac{mB^2}{3}\left(2\left(\frac{\partial u}{\partial x}\right)^2+2\left(\frac{\partial v}{\partial y}\right)^2+\left(\frac{\partial u}{\partial y}+\frac{\partial v}{\partial x}\right)^2\right)\right]\left(\frac{\partial u}{\partial x}\right),$$
$$\delta^2\left[1\ \ \delta^2\left(1\ \ 1\ \ \left(\frac{1}{\delta}+\delta\right)^2\right)\right]1, \tag{12}$$

$$\frac{S_{xy}}{\rho}=\frac{\mu_0}{\rho}\left[1+\frac{mB^2}{3}\left(2\left(\frac{\partial u}{\partial x}\right)^2+2\left(\frac{\partial v}{\partial y}\right)^2+\left(\frac{\partial u}{\partial y}+\frac{\partial v}{\partial x}\right)^2\right)\right]\left(\frac{\partial u}{\partial y}+\frac{\partial v}{\partial x}\right).$$
$$\delta^2\left[1\ \ \delta^2\left(1\ \ 1\ \ \left(\frac{1}{\delta}+\delta\right)^2\right)\right]\left(\frac{1}{\delta}\ \ \delta\right). \tag{13}$$

3 Mathematical Development

Consider the steady two-dimensional stagnation-point flow of Sutterby nanofluid toward a linear stretching sheet at $y=0$. Influences of thermophoresis and Brownian motion are considered. The fluid occupies the region $y>0$. The free stream velocity is assumed to be $U_e(x)=cx$, and the velocity of the stretching sheet is $U_w(x)=ax$, where a and c are the positive constants. The nanoparticle fraction C takes the constant value C_w, and the temperature profile becomes T_w at the wall. C_∞ and T_∞ are the ambient values of T and C, respectively. The flow diagrams of the present flow situation are the governing equations expressed as follows:

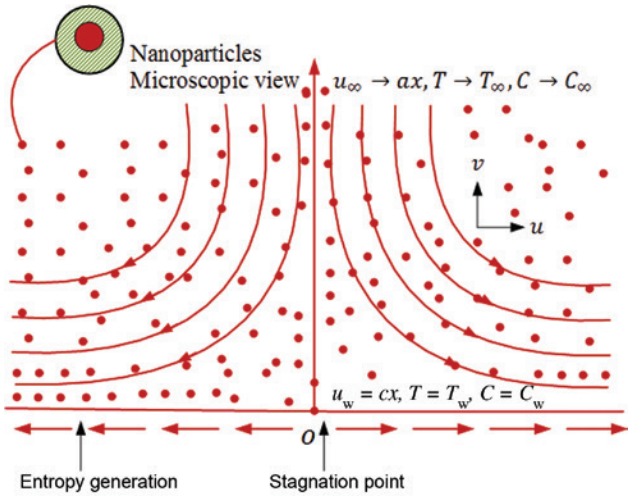

$$\frac{\partial u}{\partial x}+\frac{\partial v}{\partial y}=0, \tag{14}$$

$$u\frac{\partial u}{\partial x}+v\frac{\partial u}{\partial y}=U_e\frac{\partial U_e}{\partial x}+\frac{1}{\rho}\frac{\partial S_{xx}}{\partial x}+\frac{1}{\rho}\frac{\partial S_{xy}}{\partial y},$$
$$+g\alpha(T-T_w)+g\alpha(C-C_w), \tag{15}$$

$$u\frac{\partial v}{\partial x}+v\frac{\partial v}{\partial y}=\frac{1}{\rho}\frac{\partial S_{xy}}{\partial x}+\frac{1}{\rho}\frac{\partial S_{yy}}{\partial y}, \tag{16}$$

$$(\rho c)_f\left(\frac{\partial T}{\partial t}+u\frac{\partial T}{\partial x}+v\frac{\partial T}{\partial y}\right)=k\left(\frac{\partial^2 T}{\partial x^2}+\frac{\partial^2 T}{\partial y^2}\right)$$
$$+(\rho c)_p\left[D_B\left(\frac{\partial C}{\partial x}+\frac{\partial C}{\partial y}\right)\cdot\left(\frac{\partial T}{\partial x}+\frac{\partial T}{\partial y}\right)\right.$$
$$\left.+\frac{D_T}{T_o}\left(\frac{\partial T}{\partial x}+\frac{\partial T}{\partial y}\right)\cdot\left(\frac{\partial T}{\partial x}+\frac{\partial T}{\partial y}\right)\right], \tag{17}$$

$$\frac{\partial C}{\partial t}+u\frac{\partial C}{\partial x}+v\frac{\partial C}{\partial y}=D_B\left(\frac{\partial^2 C}{\partial x^2}+\frac{\partial^2 C}{\partial y^2}\right)+\frac{D_T}{T_0}\left(\frac{\partial^2 T}{\partial x^2}+\frac{\partial^2 T}{\partial y^2}\right). \tag{18}$$

After boundary layer assumption and inserting values of S_{xx} and S_{xy}, we have the following governing equations:

$$u\frac{\partial u}{\partial x}+v\frac{\partial u}{\partial y}=\frac{\mu_0}{\rho}\frac{\partial}{\partial y}\left[\frac{\partial u}{\partial y}+\frac{mB^2}{3}\left(\frac{\partial u}{\partial y}\right)^3\right]+g\alpha(T-T_w)+g\alpha(C-C_w), \tag{19}$$

$$u\frac{\partial T}{\partial x}+v\frac{\partial T}{\partial y}=\frac{k}{(\rho c)_f}\frac{\partial^2 T}{\partial y^2}+\frac{(\rho c)_p}{(\rho c)_f}\left[D_B\left(\frac{\partial C}{\partial y}\right)\cdot\left(\frac{\partial T}{\partial y}\right)\right.$$
$$\left.+\frac{D_T}{T_0}\left(\frac{\partial T}{\partial y}\right)\cdot\left(\frac{\partial T}{\partial y}\right)\right], \tag{20}$$

$$u\frac{\partial C}{\partial x}+v\frac{\partial C}{\partial y}=D_B\frac{\partial^2 C}{\partial y^2}+\frac{D_T}{T_0}\frac{\partial^2 T}{\partial y^2}, \tag{21}$$

with the associated boundary condition

$$u=u_w(x)=ax,\quad v=0,\quad T=T_w(x),\quad C=C_w(x)\ \text{at}\ y=0,$$
$$u=u_\infty(x)=cx,\quad u_y\to 0,\quad T\to T_\infty,\quad C\to C_\infty\ \text{as}\ y\to\infty. \tag{22}$$

In the above-mentioned equations u and v are the velocity components along the x- and y-directions, respectively. Moreover, ρ, ν, $(\rho c)_f$, $(\rho c)_p$, k, D_B, and D_T denote the fluid density, the kinematic viscosity, the heat capacity of the fluid, the effective heat capacity of the nanoparticle material, the thermal conductivity, the Brownian diffusion coefficient, and the thermophoretic diffusion coefficient, respectively. To facilitate the analysis, we introduce the subsequent conventional similarity transformation

$$u=axf'(\eta),\quad v=-\sqrt{a\nu}f(\eta),\quad \eta=y\sqrt{\frac{a}{\nu}},$$
$$\theta(\eta)=\frac{T-T_w}{T_\infty-T_w},\quad \phi(\eta)=\frac{C-C_w}{C_\infty-C_w}. \tag{23}$$

On substituting (23) into (19)–(22) and taking constant pressure, we have the following system of ordinary differential equations

$$f'''+ff''-f'^2+\frac{m}{2}\mathrm{ReDe}f''^2f'''+\mathrm{Gr}\theta+\mathrm{Br}\phi+A^2=0, \tag{24}$$

$$\theta''+\mathrm{Pr}\,f\theta'+\mathrm{Pr}N_b\theta'\phi'+\mathrm{Pr}N_t\theta'^2=0, \tag{25}$$

$$\phi''+\mathrm{Sc}f\phi'+\frac{N_t}{N_b}\theta''=0, \tag{26}$$

$$f(0)=0,\ f'(0)=1,\ \theta(0)=1,\ \phi(0)=1,\quad f'(\infty)\to A,\ \theta(\infty)\to 0,\ \phi(\infty)\to 0. \tag{27}$$

Where primes represent the differentiation with respect to η, and Gr is the local temperature Grashof number, Br is the local nanoparticle Grashof number, Re is the Reynolds number, De is the Deborah number, and m is the power law index. Pr, Sc, N_b, and N_t denotes the Prandtl number, the Schmidt number, the Brownian motion parameter, and thermophoresis parameter, respectively, and defined as

$$\mathrm{Re}=\frac{ax^2}{\nu},\ \mathrm{De}=\frac{B^2a^2}{\nu},\ \mathrm{Gr}=g\alpha(T_\infty-T_w),\ \mathrm{Br}=g\alpha(C_\infty-C_w),$$
$$\mathrm{Pr}=\frac{\nu(\rho c)_f}{k},\ \mathrm{Sc}=\frac{\nu}{D_B},\ A=\frac{c}{a},\ N_b=\frac{(\rho c)_pD_B(C_\infty-C_w)}{(\rho c)_f\nu},$$
$$N_t=\frac{(\rho c)_pD_T(T_\infty-T_w)}{(\rho c)_fT_\infty\nu}. \tag{28}$$

The skin friction coefficient C_f, the local Nusselt number Nu_x, and the local Sherwood number Sh_x are given by

$$C_f=\frac{\tau_w}{\rho u_w^2(x)},\quad \mathrm{Nu}_x=\frac{xq_w}{k(T_w-T_\infty)},\quad \mathrm{Sh}_x=\frac{xC_w}{D_B(C_w-C_\infty)}, \tag{29}$$

or

$$\mathrm{Re}_x^{\frac{1}{2}}C_f=-\left[f''(0)+\frac{m}{6}\mathrm{DeRe}(f''(0))^3\right],\quad \mathrm{Re}_x^{-\frac{1}{2}}\mathrm{Nu}_x=-\theta'(0),$$
$$\mathrm{Re}_x^{-\frac{1}{2}}\mathrm{Sh}_x=-\phi'(0), \tag{30}$$

where $\mathrm{Re}_x=ax^2/\nu$ is the local Reynolds number based on stretching velocity $u_w(x)$.

4 Entropy Generation Analysis

Heat transfer to fluid flow with apparent viscosity in a channel is irreversible. Hence, entropy production gets to be persistent because of the exchange of energy and momentum within fluid particles in channel. The expression for the total entropy generation within fluid system has been defined by [10, 17–29]:

$$S_G=\frac{k}{T_0}\left(\left(\frac{\partial T}{\partial x}\right)^2+\left(\frac{\partial T}{\partial y}\right)^2\right)+\tau\cdot L. \tag{31}$$

The nondimensional form of entropy generation due to fluid friction becomes

$$\mathrm{Ns}=\frac{S_G}{S_{G_0}}=\left(\frac{\partial\theta}{\partial\eta}\right)^2+\frac{\mathrm{Br}\gamma}{\Lambda}\left[1+\frac{m\mathrm{ReDe}}{3}(f'')^2\right](f'')^2, \tag{32}$$

where Ns is a nondimensional quantity termed as entropy generation number, which is the ratio of the actual entropy generation rate S_G to the characteristic entropy transfer rate S_{G_0}. The first term of Ns represents the heat dissipation and can be assigned as N_H, and the second term is due to viscous dissipation termed as N_F, i.e.

$$\mathrm{Ns}=N_H+N_F,$$
$$N_H=\left(\frac{\partial\theta}{\partial\eta}\right)^2,$$
$$N_F=\frac{\mathrm{Br}\gamma}{\Lambda}\left[1+\frac{m\mathrm{ReDe}}{3}(f'')^2\right](f'')^2. \tag{33}$$

Alternatively, another irreversibility parameter Bejan number Be is defined as

$$\mathrm{Be}=\frac{N_H}{\mathrm{Ns}}. \tag{34}$$

5 The Numerical Solutions

The solution of (24)–(26) along with boundary conditions in (27) is computed by using a numerical technique known as the shooting method. Here we convert nonlinear equations into the system of seven first-order ordinary differential equations by labeling variables, i.e. $f=y_1$, $f'=y_1'=y_2$, $f''=y_2'=y_3$, $f'''=y_3'$, $\theta=y_4$, $\theta'=y_4'=y_5$, $\theta''=y_5'$, $\phi=y_6$, $\phi'=y_6'=y_7$, $\phi''=y_7'$. Then we solved it by using the RK method of order 5. The iterative process will be terminated when the error involved is $<10^{-6}$.

6 Results and Discussion

To understand the physical properties of the problem, we have investigated the effects of different parameters

on fluid flow, temperature, and concentration profiles through graphs and tables. Figure 1 displays the effect of stretching parameter A. It can be seen that the velocity profile increases with the increasing values of A. Here we examined the influence of stretching parameter ($A = c/a$) for the case when free stream velocity is less than the stretching ratio. Obviously, for the present scenario, velocity increases for smaller stretching rate. Figures 2 and 3 demonstrate the behavior of the local nanoparticle Grashof number Br and the local temperature Grashof number Gr on fluid velocity, respectively. As the Grashof number is the ratio of buoyancy to viscous forces, a reasonable increase in the Grashof number results in weaker viscous forces. Hence, the boundary layer thickness increases. As the Reynolds number Re is the ratio of inertial forces to viscous force, this means an increase in Reynolds number reduces viscous forces. Figures 4 and 5 display the shear thinning ($m < 0$) and the shear thickening ($m > 0$) behavior of Reynolds number. In the shear thinning case for high Reynolds number, viscous forces decrease and as a result fluid velocity reduces, whereas in the shear thickening case, opposite behavior is formed because viscous forces decrease and velocity increases. The Deborah number De is used in rheology to characterize the fluidity of materials under specific flow conditions. The velocity profile corresponding to the Deborah number lessens for shear thinning fluid (see Fig. 6), and it enhances when fluid is shear thickening (see Fig. 7). The contribution of power law index m is depicted in Figure 8, where $m = -1$ corresponds to shear thinning fluid, $m = 0$ is a Newtonian fluid, and $m = 1$ displays shear thickening fluid.

Figures 9 and 10 give the effects of the Brownian motion N_b and thermophoresis parameters N_t on temperature profile $\theta(\eta)$, respectively. Both figures elucidate that temperature profile as well as thermal boundary layer thickness increases with the increasing N_b and N_t. The increase in N_b and N_t corresponds to the increase in the Brownian diffusion coefficient and thermophoretic diffusion coefficient, respectively. Both physical phenomena are well known in significantly affecting the thermal conductivity of nanofluids. Figure 11 depicts that as the Prandtl number Pr increases, the mass concentration also increases. Prandtl number is the ratio of kinematic viscosity to thermal conductivity, the increase in Pr corresponds to the decrease in thermal conductivity and the increase in fluid viscosity, which leads to the increase in nanoparticle concentration. However, increasing values of Schmidt number Sc contribute in nanoparticle concentration in an opposite manner, as shown in Figure 12. This happens mainly because of the fact that the Schmidt number is the ratio of kinematic viscosity to the Brownian diffusion coefficient, and an increase in Sc is due to a decrease in the Brownian diffusion coefficient, which plays a vital role in lowering nanoparticle concentration. There would be a significant reduction in concentration boundary layer when Sc is increased. It is observed that the effect of N_b on the nanoparticle concentration profile $\phi(\eta)$ is opposite to that of temperature profile $\theta(\eta)$, as plotted in Figure 13. It is apparent from Figure 13 that mass concentration is decreasing as N_b is increasing. It seems that the Brownian motion parameter acts to increase thermal boundary layer and at the same time exacerbates particle deposition away from fluid regime to surface, which results in a decrease in the concentration boundary layer thickness. Figure 14 is plotted for variation in N_t. It can be viewed that increasing values of thermophoresis parameter enhance mass concentration. This is because the increase in N_t corresponds to the increase in thermophoretic diffusion coefficient, enhancing mass concentration.

The variation in total entropy generation number Ns is shown against η for different parameters in Figures 15–19. In Figures 15 and 16, the effect of the Deborah number on entropy generation number has been examined, which shows that there is an increase in entropy generation number near the wall for shear thickening fluid and decrease near the wall for shear thinning fluid. A similar behavior for Reynolds number in entropy generation can be seen for shear thinning and shear thickening fluids (see Figs. 17 and 18). Figure 19 depicts that the ($m < 0$) entropy generation for shear thinning fluid, the ($m = 0$) Ns for the Newtonian fluid, and the ($m > 0$) entropy generation for shear thickening fluid have a significant increase in Ns when compared with Newtonian and shear thinning fluids. The Bejan number Be is defined as

$$\mathrm{Be} = \frac{\text{Entropy generation due to heat transfer}}{\text{Total entropy generation}}.$$

The Bejan number ranges from 0 to 1, and when entropy generation due to heat transfer is dominant, Be is close to 1. Figures 20–24 represent the behavior of different physical parameters on the Bejan number. It can be analyzed that the Bejan number decreases with the Deborah and Reynolds number for dilatant and increases for both numbers for pseudoplastic fluids. Figure 24 demonstrates the variation of m for the three classifications.

Table 1 represents the effect of dimensionless parameter Gr, Br, A, m, Re, and De on numerical values of skin friction. It is observed that the values of $\mathrm{Re}_x^{-\frac{1}{2}} C_f$ decreases as the values of these parameters increase. $m < 0$ shows

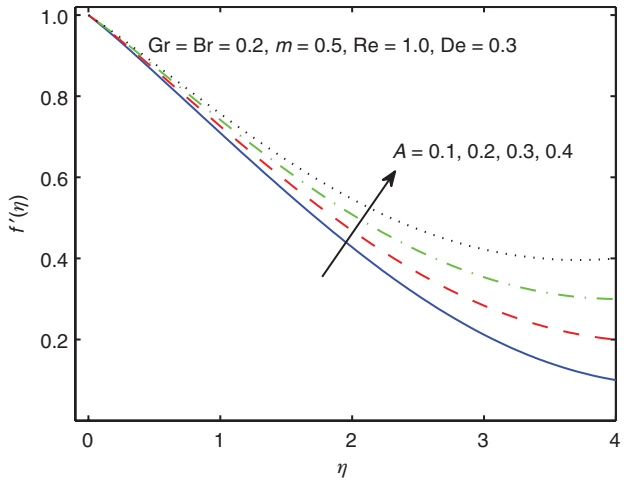

Figure 1: Impact of A on $f'(\eta)$.

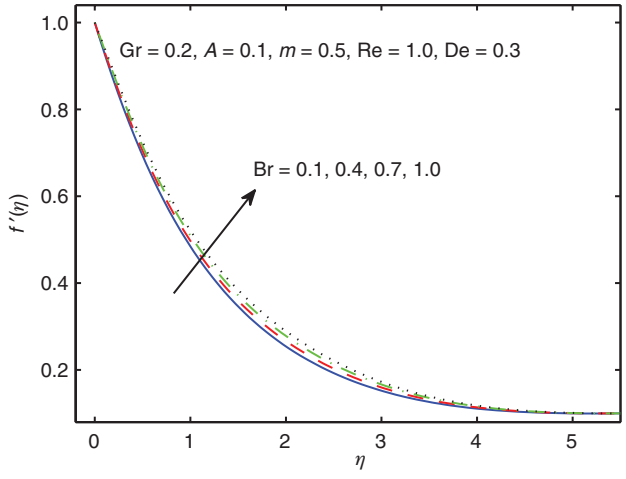

Figure 2: Impact of Br on $f'(\eta)$.

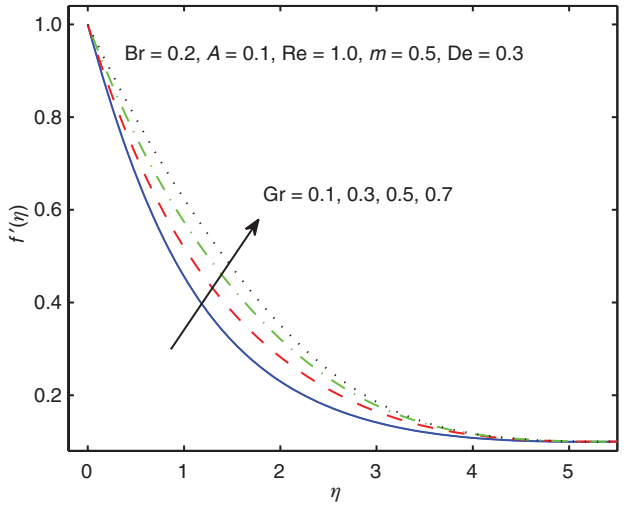

Figure 3: Impact of Gr on $f'(\eta)$.

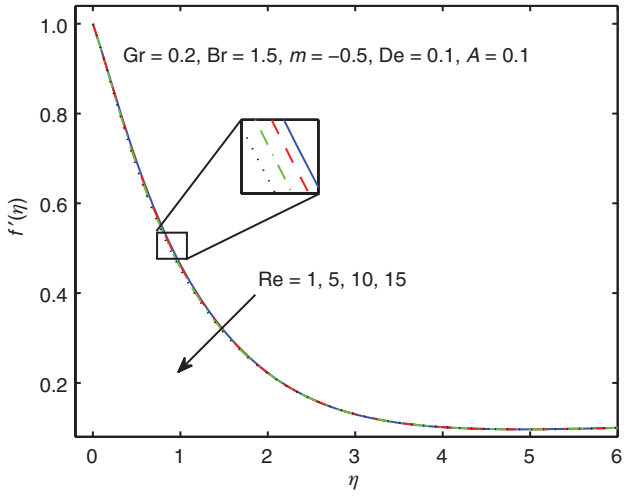

Figure 4: Impact of Re on $f'(\eta)$ for shear thinning fluid.

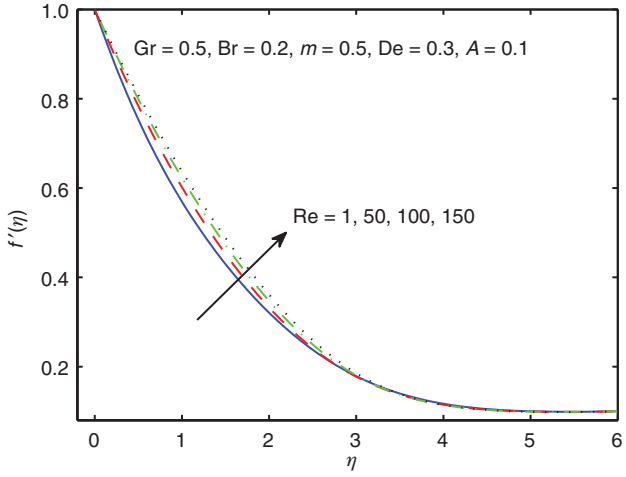

Figure 5: Impact of Re on $f'(\eta)$ for shear thickening fluid.

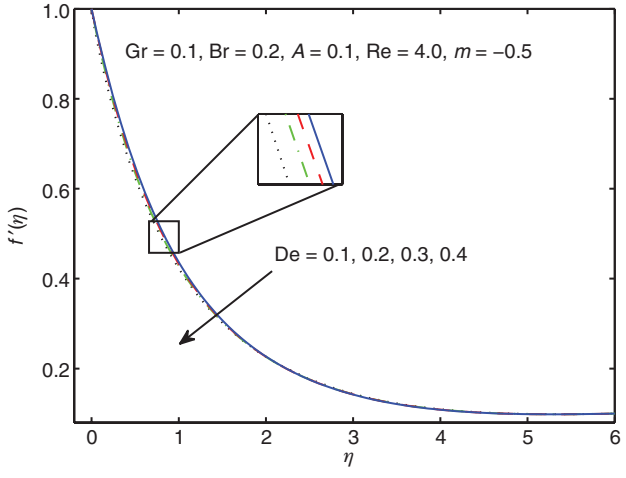

Figure 6: Impact of De on $f'(\eta)$ for shear thinning fluid.

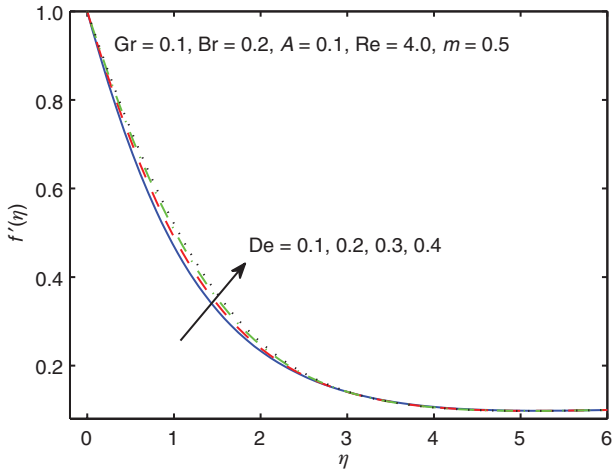

Figure 7: Impact of De on $f'(\eta)$ for shear thickening fluid.

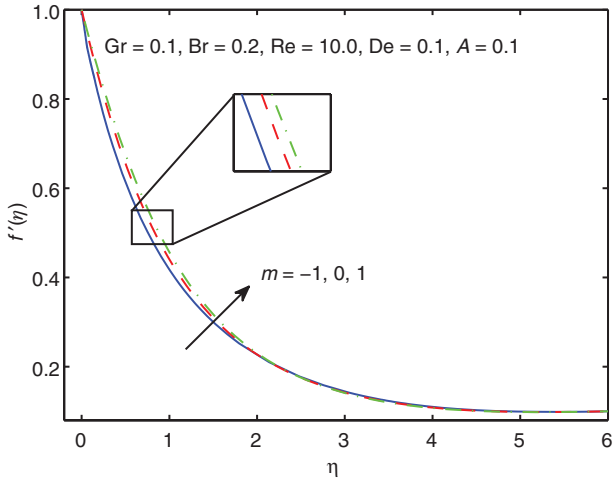

Figure 8: Impact of m on $f'(\eta)$.

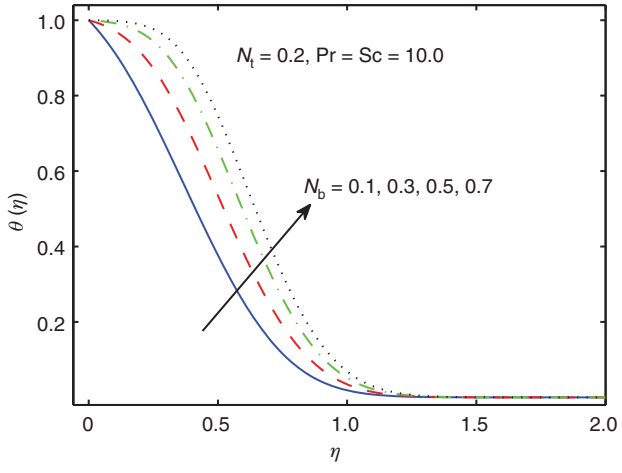

Figure 9: Impact of N_b on $\theta(\eta)$.

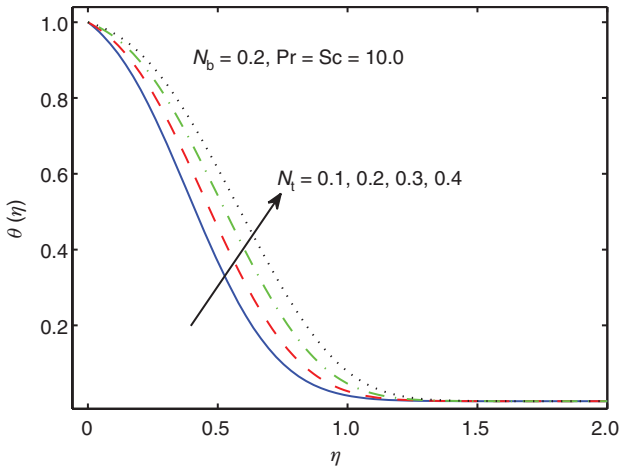

Figure 10: Impact of N_t on $\theta(\eta)$.

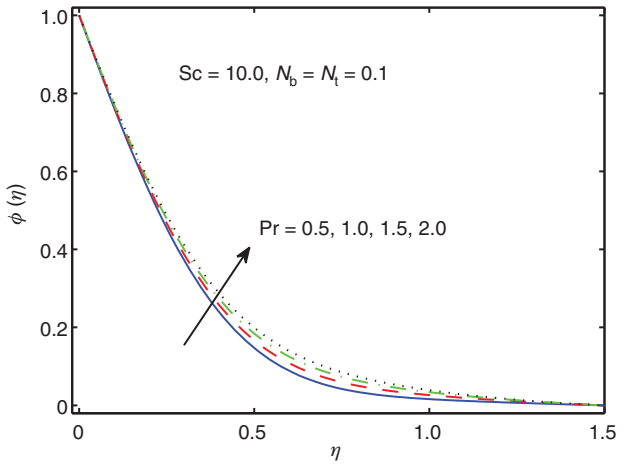

Figure 11: Impact of Pr on $\theta(\eta)$.

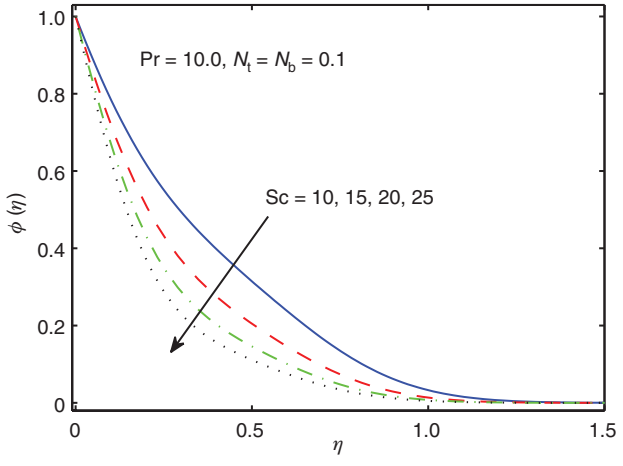

Figure 12: Impact of Sc on $\theta(\eta)$.

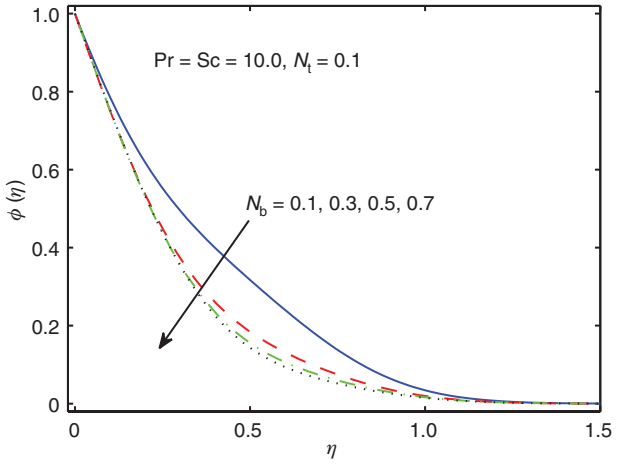

Figure 13: Impact of N_b on $\phi(\eta)$.

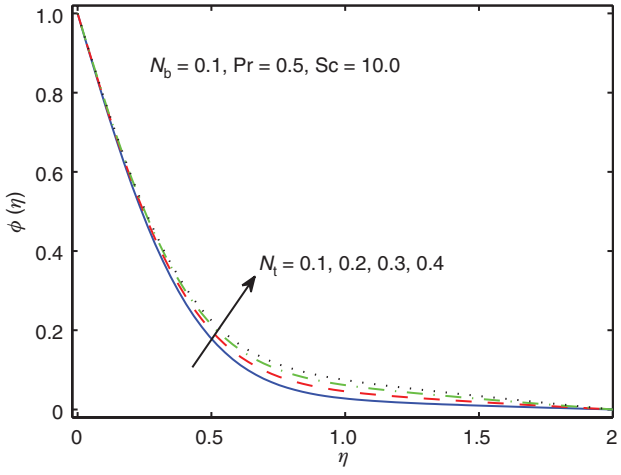

Figure 14: Impact of N_t on $\phi(\eta)$.

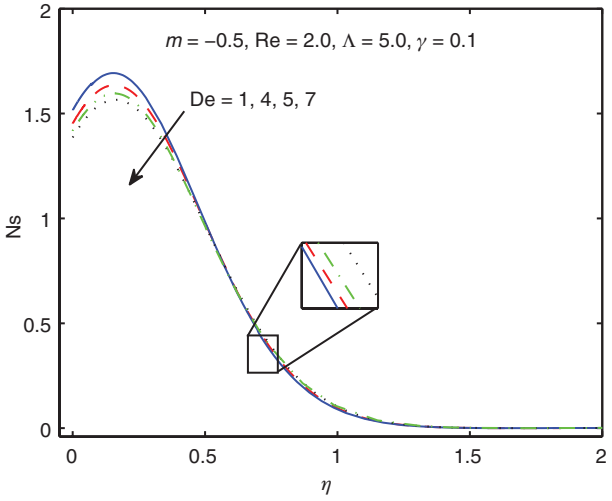

Figure 15: Impact of De on Ns for shear thinning fluid.

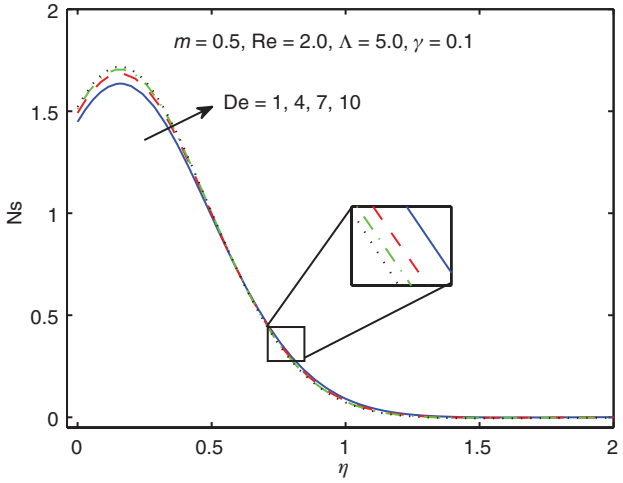

Figure 16: Impact of De on Ns for shear thickening fluid.

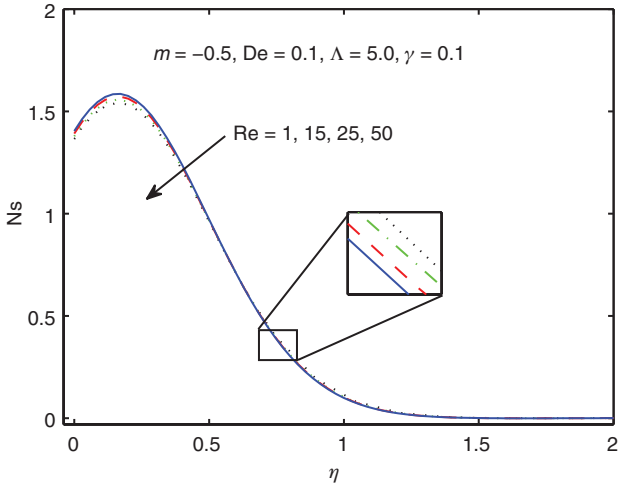

Figure 17: Impact of Re on Ns for shear thinning fluid.

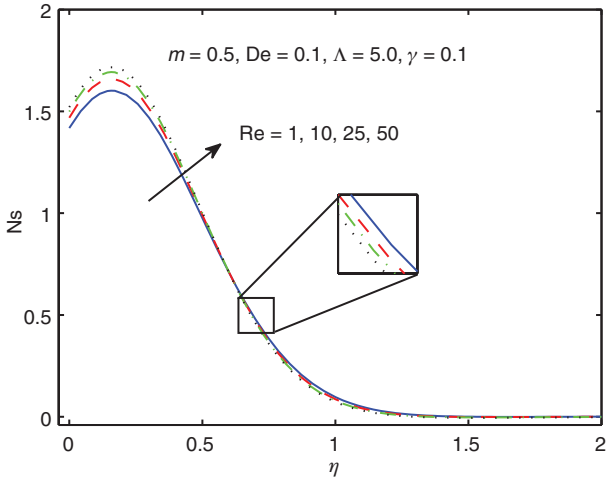

Figure 18: Impact of Re on Ns for shear thickening fluid.

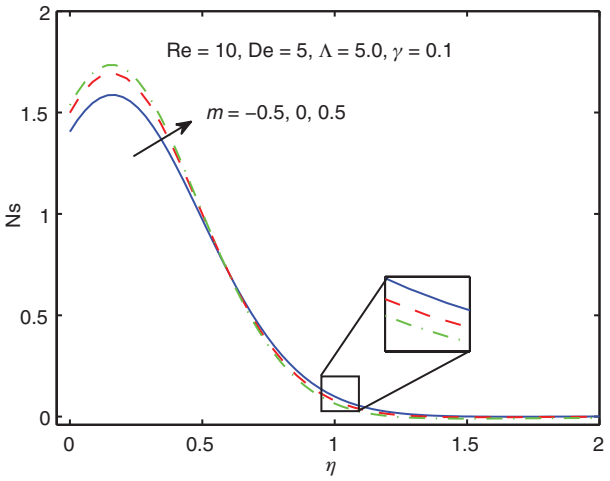

Figure 19: Impact of m on Ns.

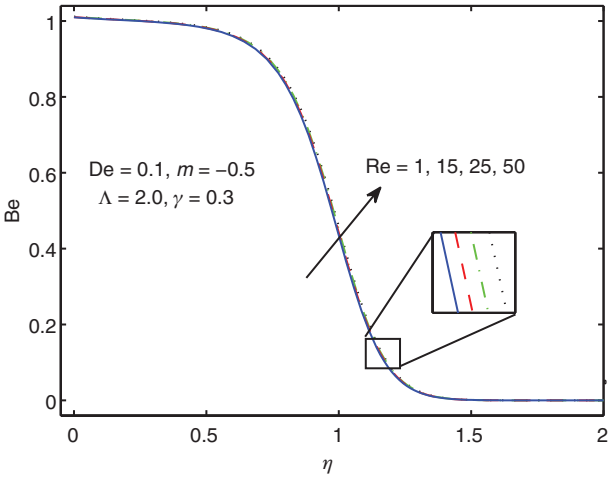

Figure 22: Impact of Re on Be for shear thinning fluid.

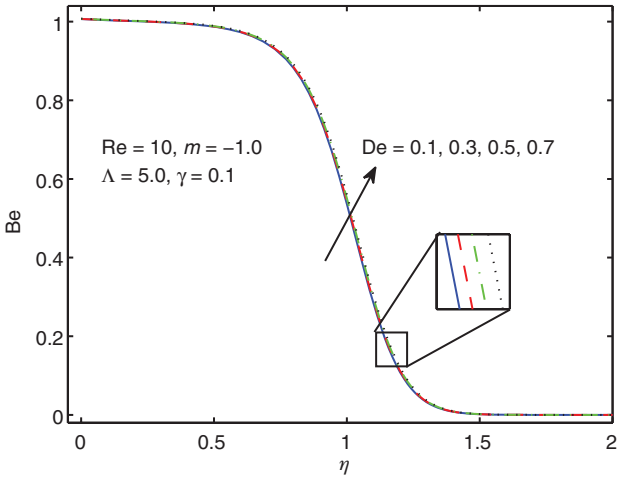

Figure 20: Impact of De on Be for shear thinning fluid.

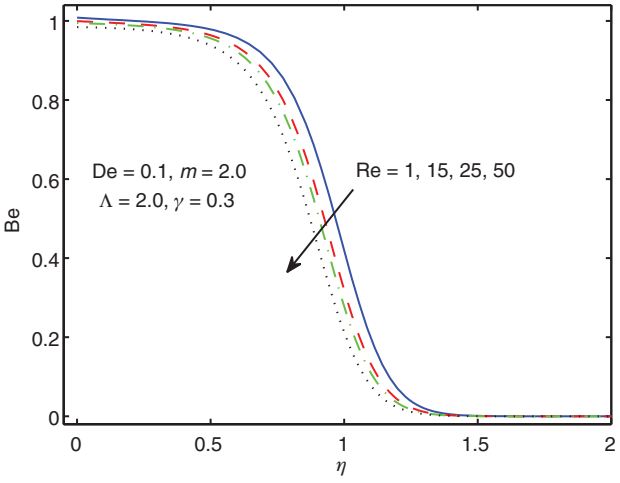

Figure 23: Impact of Re on Be for shear thickening fluid.

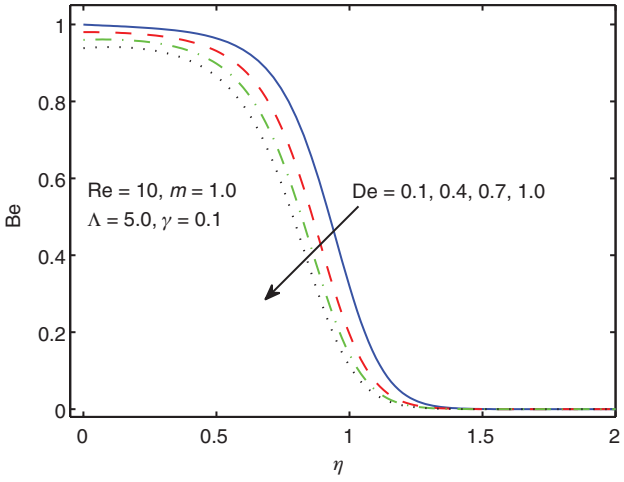

Figure 21: Impact of De on Be for shear thickening fluid.

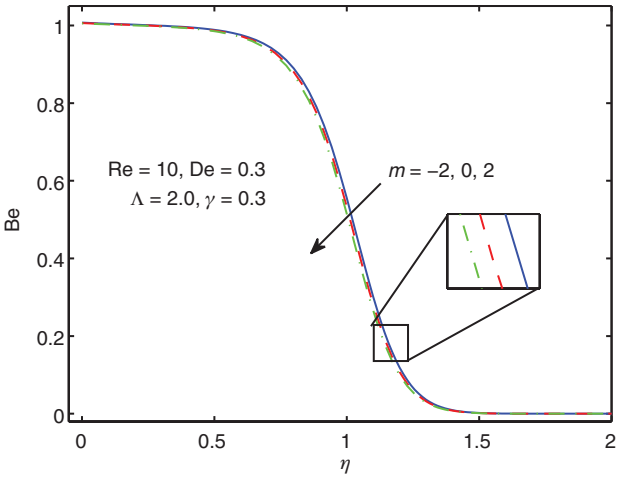

Figure 24: Impact of m on Be.

Table 1: Computational results of coefficient of skin friction for the different values of significant parameters.

Gr	Br	A	m	Re	De	$\mathrm{Re}_x^{-\frac{1}{2}} C_f$
0.1	0.5	0.1	0.5	1.0	0.3	0.5486
0.3						0.4882
0.5						0.4282
0.7						0.3684
0.3	0.4					0.5712
	0.3					0.6532
	0.2					0.7340
	0.1					0.8136
	0.2	0.2				0.6949
		0.3				0.6564
		0.4				0.6187
		0.5				0.5816
		0.1	−0.5			0.7579
			0.0			0.7451
			0.5			0.7340
			1.0			0.6369
			0.5	2.0		0.7242
				3.0		0.7154
				4.0		0.7074
				5.0		0.7000
				2.0	0.1	0.7376
					0.3	0.7242
					0.5	0.7126
					0.7	0.7024

Table 2: Numerical results of local heat and concentration flux.

N_t	N_b	Pr	Sc	$\mathrm{Re}_x^{-\frac{1}{2}} \mathrm{Nu}_x$	$\mathrm{Re}_x^{-\frac{1}{2}} \mathrm{Sh}_x$
0.1	0.2	10.0	10.0	0.5134	2.4377
0.2				0.3700	2.5889
0.3				0.2755	2.7482
0.4				0.2118	2.8938
0.2	0.1			0.7029	2.3769
	0.3			0.1838	2.5794
	0.5			0.0395	2.5041
	0.7			0.0075	2.4536
	0.2	5.0		0.5663	2.3781
		10.0		0.3700	2.5889
		15.0		0.2224	2.7215
		20.0		0.1306	2.7955
		10.0	1.0	0.9903	1.0437
			2.0	0.8128	1.8837
			3.0	0.6851	2.4349
			4.0	0.5944	2.8683

the values of skin frictions for pseudoplastic, $m > 0$ for dilatant fluids, and $m = 0$ for the case of the Newtonian fluid. The tabulated values of rate of heat flux and rate of mass concentration for increasing values of N_t, N_b, Pr, and Sc are shown in Table 2. The increasing values of all these parameter enhance the Sherwood number, whereas for the rate of heat flux, an opposite behavior can be seen. Table 3 illustrates the numerical results for N_H, N_F, and Ns for the different values of important parameters. It is observed that values of heat dissipation N_H increase, and viscous dissipation N_F and entropy generation Ns decrease with the increase in power law index m, Reynolds number Re, and Deborah number De. A constant behavior can be seen for heat dissipation N_H corresponding to γ and Λ. The values of viscous dissipation N_F and entropy generation Ns decrease for increasing values of γ and increase as Λ increases. Table 4 shows the comparison of numerical values of Nusselt number with the results of Wang [30], Gorla and Sidawi [31], Khan and Pop [32], and Makinde and Aziz [33] in the limiting sense. An excellent agreement is observed among all the results.

Table 3: Numerical results of entropy generation for distinct values of pertinent parameters.

m	Re	De	γ	Λ	N_H	N_F	Ns
−2.0					1.2947	−0.7059	0.5888
−1.0					1.3060	−0.7266	0.5794
0.0					1.3151	−0.7451	0.5699
1.0					1.3227	−0.7622	0.5605
2.0					1.3292	−0.7781	0.5511
1.0	3.0				1.3350	−0.7933	0.5418
	5.0				1.3448	−0.8216	0.5232
	7.0				1.3529	−0.8480	0.5048
	9.0				1.3597	−0.8731	0.4866
	10.0	0.5			1.3789	−0.9611	0.4178
		0.7			1.3901	−1.0316	0.3581
		0.9			1.3985	−1.0991	0.2993
		1.1			1.4050	−1.1648	0.2402
		0.1	0.2		1.3368	−1.5963	−0.2595
			0.3		1.3368	−2.3944	−1.3944
			0.1	0.2	1.3368	−0.3991	0.9377
				0.3	1.3368	−0.2660	1.0707

Table 4: Comparison of values of Nusselt Number $-\theta'(0)$ with those of Wang [30], Gorla and Sidawi [31], Khan and Pop [32], and Makinde and Aziz [33] when $A = N_t = N_b = \mathrm{Gr} = \mathrm{Br} = 0.0$, and $m = 0.0$.

Pr	[30]	[31]	[32]	[33]	Present
0.07	0.0663	0.0663	0.0663	0.0663	0.0663
0.20	0.1691	0.1691	0.1691	0.1691	0.1691
0.70	0.4539	0.4539	0.4539	0.4539	0.4539
2.00	0.9113	0.9113	0.9113	0.9113	0.9113
7.00	1.8954	1.8954	1.8954	1.8954	1.8954
20.00	6.4621	6.4621	6.4621	6.4621	6.4621

7 Conclusion

From the previous section after the graphical and computational results and discussion on the behavior of several physical parameters, eminent findings are enlisted as follows:

- The ratios of inertial to viscous forces and characteristic parameter of the fluidity of fluid contribute oppositely in shear thinning and shear thickening fluids.
- Thermal boundary layer enhances for the Brownian motion parameter and N_t, whereas mass concentration boundary layer shows the opposite behavior of N_b.
- Prandlt and Schmidt numbers affect mass concentration reversely.
- For De and Re, entropy generation number behavior is opposite to each other for shear thinning and thickening fluids, respectively.
- Ns increases near the stretching sheet for variation is the power law index, while a reverse pattern is observed afterward.
- De and Re affect irreversibility parameter in an opposite manner for shear thinning and thickening fluids, respectively.
- Coefficient of skin friction is observed to decay for all significant parameters.
- Contribution of pertinent parameters is opposite for Nu_x number as compared with Schmidt number.
- Power law index, Re, and De increase the contribution of heat dissipation and decrease viscous dissipation in entropy generation number.
- γ decreases viscous dissipation, whereas Λ increases it.

Nomenclature

a, c, f	positive constants and dimensionless component of velocity
p, c_p	pressure and specific heat
Gr, Br	local temperature and nanoparticle Grashof numbers
N_t, N_b	thermophoresis and Brownian motion parameters
De, Sc, Re	Deborah, Schmidt, and Reynolds numbers, respectively
D_B, D_T	Brownian and thermophoretic diffusion coefficients respectively
$(\rho c)_f, (\rho c)_p$	heat capacity and effective heat capacity
B, S	material constant and Extra stress tensor
k, m	thermal conductivity and power law index
τ_w, q_w	shear stress and heat flux at wall
Pr, A	Prandtl number and stretching ratio parameter
C, C_w, C_∞	nanoparticle fraction, wall and ambient fractions respectively
T, T_w, T_∞,	fluid temperature, wall and ambient temperatures respectively
$C_f, \mathrm{Nu}_x, \mathrm{Sh}_x$	skin friction coefficient, local Nusselt and Sherwood numbers
S_G, S_{G_0}	entropy generation rate and characteristic entropy transfer rate
Ns, Be	entropy generation and Bejan numbers
N_H, N_F	heat and viscous dissipations
u, v	velocity components in x and y-directions
x, y	Cartesian coordinates

Greek symbols

η	dimensionless space variable
ϕ	dimensionless concentration
θ	dimensionless temperature
ν, μ_0	kinematic and dynamic viscosities
ρ	fluid density
τ	stress tensor

Subscripts

w	wall conditions
∞	conditions at infinity

References

[1] R. L. Batra and M. Eissa, Polym. Plast. Technol. Eng. **33**, 489 (1994).
[2] B. C. Sakiadis, AIChE J. **7**, 26 (1961).
[3] V. Lyubimov and A. V. Perminov, J. Eng. Phys. Thermophys. **75**, 92 (2002).
[4] T. Hayat, Z. Iqbal, M. Mustafa, and S. Obaidat, Heat Transfer Asian Res. **40**, 744 (2011).
[5] S. Nadeem, S. T. Hussain, and C. Lee, Braz. J. Chem. Eng. **30**, 619 (2013).
[6] T. Hayat, Z. Iqbal, and M. Mustafa, J. Mech. **28**, 209 (2012).
[7] B. Bidin and R. Nazar, Eur. J. Sci. Res. **33**, 710 (2009).
[8] S. U. S. Choi, Enhancing thermal conductivity of fluids with nanoparticles. Developments and applications of non-Newtonian flows FED-vol. 231/MD-vol. 66, 99 (1995).
[9] J. Buongiorno, ASME J. Heat Transfer **128**, 240 (2006).
[10] A. Malvandi and D. D. Ganji, Int. J. Therm. Sci. **84**, 196 (2014).
[11] K. Hiemenz, Dinglers Polytech. J. **326**, 321 (1911).
[12] T. C. Chiam, J. Phys. Soc. Jpn. **63**, 2443 (1994).
[13] W. A. Khan and I. Pop, Comm. Nonlinear Sci. Num. Simul. **15**, 3435 (2010).
[14] Y. Zhong and T. Fang, Int. J. Heat Mass Transfer **54**, 3103 (2011).
[15] K. Bhattacharyya and K. Vajravelu, Comm. Nonlinear Sci. Num. Simul. **17**, 2728 (2012).
[16] A. Malvandi, Therm. Sci. **19** 1603 (2015).
[17] A. Malvandi, F. Hedayati, and D. D. Ganji, Powder Tech. **253**, 377 (2014).
[18] A. R. Falahat, Int. J. Med. Sci. Educ. **2**, 44 (2011).
[19] L. Jie and K. Clement, J. Heat Transfer **132**, 122401 (2010).
[20] M. R. Hassan, R. Sadri, G. Ahmadi, M. B. Dahari, S. N. Kazi, et al., Entropy **15**, 144 (2013).

[21] O. Mahian, A. Kianifar, C. Kleinstreuer, M. A. Al-Nimr, I. Pop, et al., Int. J. Heat Mass Transfer **65**, 514 (2013).
[22] A. Malvandi, D. D. Ganji, F. Hedayati, and E. Yousefi Rad, Alex. Eng. J. **52**, 595 (2013).
[23] S. Chen and Z. Tian, Int. J. Thermal Sci. **49**, 2211 (2010).
[24] A. Bejan, Entropy Generation Minimization, CRC Press, Boca Raton, FL 1996.
[25] L. Erbay, M. Yalcin and M. Ercan, Heat Mass Transfer **43** (2007) 729.
[26] A. Malvandi, A. Ghasemi, and D. D. Ganji, Int. J. Thermal Sci. **109**, 10 (2016).
[27] A. Malvandi and D. D. Ganji, Euro. J. Mech. B. Fluids **52**, 169 (2015).
[28] A. Malvandi, S. A. Moshizi, E. G. Soltani, and D. D. Ganji, Comp. Fluids **89**, 124 (2014).
[29] J. A. Falade, S. O. Adesanya, J. C. Ukaegbu, and M. O. Osinowo, Alex. Eng. J. **55**, 69 (2016).
[30] C. Y. Wang, J. Appl. Math. Mech. (ZAMM) **69**, 418 (1989).
[31] R. S. R. Gorla and I. Sidawi, Appl. Sci. Res. **52**, 247 (1994).
[32] W. A. Khan and I. Pop, Int. J. Heat Mass Transfer **53**, 2477 (2010).
[33] O. D. Makinde and A. Aziz, Int. J. Thermal Sci. **50**, 1326 (2011).